Monthly Notices
of the
ROYAL ASTRONOMICAL SOCIETY

Mon. Not. R. Astron. Soc. **415,** 1849–1863 (2011) doi:10.1111/j.1365-2966.2011.18818.x

Prospects of observing continuous gravitational waves from known pulsars

Matthew Pitkin★

SUPA, School of Physics and Astronomy, University of Glasgow, University Avenue, Glasgow G12 8QQ

Accepted 2011 March 30. Received 2011 March 24; in original form 2011 February 14

ABSTRACT

Several past searches for gravitational waves from a selection of known pulsars have been performed with data from the science runs of the Laser Interferometer Gravitational-Wave Observatory (LIGO) gravitational wave detectors. So far these have led to no detection, but upper limits on the gravitational wave amplitudes have been set. Here we study our intrinsic ability to detect, and estimate the gravitational wave amplitude for non-accreting pulsars. Using spin-down limits on emission as a guide we examine amplitudes that would be required to observe known pulsars with future detectors (Advanced LIGO, Advanced Virgo and the Einstein Telescope), assuming that they are triaxial stars emitting at precisely twice the known rotation frequency. Maximum allowed amplitudes depend on the stars' equation of state (e.g. a normal neutron star, a quark star, a hybrid star) and the theoretical mass quadrupoles that they can sustain. We study what range of quadrupoles, and therefore equation of state (EoS), would be consistent with being able to detect these sources. For globular cluster pulsars, with spin-downs masked by accelerations within the cluster, we examine what spin-down values gravitational wave observations would be able to set. For all pulsars we also alternatively examine what internal magnetic fields they would need to sustain observable ellipticities.

Key words: gravitational waves – stars: neutron – pulsars: general.

1 INTRODUCTION

Just under 2000 pulsars are currently known (Manchester et al. 2005) and these provide enticing targets to search for continuous gravitational wave emission. Searches for gravitational waves from known pulsars (Abbott et al. 2005, 2007a, 2010) estimate four unknown parameters: the gravitational wave amplitude h_0, the initial phase relative to the electromagnetic pulse phase ϕ_0, the cosine of the orientation angle $\cos\iota$ and the polarization angle ψ. As yet no signal has been seen from any pulsar, so observations provide no constraints on these parameters other than an upper limit on h_0. However, with detector sensitivities improving over the next few years we will be beating spin-down based upper limits for many pulsars. This gives us the potential of direct gravitational wave detection (if gravitational waves provide a braking mechanism that is comparable to the electromagnetic braking), therefore allowing us to place real constraints on these parameters. The h_0 parameter in particular will allow us to say something about the make up of the neutron star[1] itself as it is related to the star's mass quadrupole moment, and therefore the equation of state (EoS). Some discussion of useful astrophysics that could be gained from measuring $\cos\iota$ is given in Jones (2007), and accurate polarization measurements could provide limits on, or allow the study of, different theories of gravity (see e.g. Will 2006), but here we will concentrate on the amplitude and quadrupole measurement. It is important to stress that there is much that is unknown about neutron stars and whether they can produce and sustain large enough quadrupoles to be observable via gravitational waves, so explaining such issues is still an area of great interest. In this study we only discuss prospects for observing non-accreting pulsars. In accreting systems different gravitational wave emission mechanism may be present, and the links between electromagnetic observations and any gravitational wave signal are less well known. Watts et al. (2008) provide a good study of detection prospects for accreting neutron stars.

1.1 Searches for known pulsars

Since the start of science data taking from the current generation of interferometric gravitational wave detectors (LIGO, GEO 600, TAMA and Virgo; Abbott et al. 2004a; Ando et al. 2005; Acernese et al. 2008) searches looking for gravitational waves from a large selection of *known* pulsars (millisecond and young pulsars with spin frequencies greater than ∼20 Hz) have been performed (Abbott et al. 2005, 2007a, 2010). In the most recent analysis 116 pulsars were searched for using approximately a year and a half of data from each of the three LIGO detectors (Abbott et al. 2010), which were operating at their design sensitivity (Abbott et al. 2009a).

★E-mail: matthew.pitkin@glasgow.ac.uk

[1] We will use 'neutron star' as a generic term for all types of compact star used in this paper, unless specifically stated.

Unfortunately, no signal was seen from any of these objects, but for the majority the sensitivity was still well above, by factors of 10 to over 100 times, their spin-down limits. The spin-down limit is set by assuming that the star's spin-down luminosity is equal to its gravitational wave luminosity, i.e. all the rotational energy lost by the pulsar is due to radiation via gravitational waves from the Q_{22} mass quadrupole. This limit does require one to assume a moment of inertia for the star, generally taken as the canonical value of 10^{38} kg m^2 (or 10^{45} g cm^2 in cgs units), and that its distance is precisely known. For one object, the Crab pulsar, this limit has been passed (Abbott et al. 2008a, 2010) although still no gravitational waves were seen, and for four others the upper limit obtained was within a factor of 10 from spin-down.

For known pulsars the parameter space to be searched over is comparatively small (position and phase evolution are known) and long observation times can be used in a coherent way. This makes such searches more sensitive than semi-targeted, or blind searches for similar sources (Abbott et al. 2007b, 2008b, 2009b,c), although potentially will miss out on some interesting, but currently unknown, objects. Knispel & Allen (2008) discuss the potential strength of a population of gravitational wave emitting Galactic neutron stars. Here, we therefore concentrate our study on estimating the prospects for fully targeted searches.

The paper is set out as follows. In Section 2 we will assess the potential signal-to-noise ratios (S/N) at which currently known pulsars could be observed with future detectors, review a detection statistic for these pulsars, and demonstrate the parameter estimation capabilities of the standard search technique at a variety of S/N; in Section 3 we review some estimates of the maximum quadrupole moments for neutron stars given a selection of EoS; in Section 4 we assess the potential signals, and associated quadrupoles, observable in future detectors based on spin-down limits and limits on our sensitivity, and how these limits can be thought of in terms of internal magnetic field strengths, and for globular cluster (GC) pulsar limits on their spin-down. Parts of this work are similar in scope to the review by Owen (2006), and the discussions in Abbott et al. (2007b) and Andersson et al. (2011).

2 ESTIMATING SIGNALS IN FUTURE DETECTORS

The next (second) generation of interferometric gravitational wave detectors, such as Advanced LIGO (aLIGO) (Harry et al. 2010), Advanced Virgo (AdvVirgo) (The Virgo Collaboration 2009), the Large-scale Cryogenic Gravitational Wave Telescope (LCGT) (Kuroda 2010) and GEO-HF (Willke 2006), expect to provide order of magnitude sensitivity improvements over current detectors, and offer the opportunity to beat spin-down limits for nearly 60 pulsars (see Section 2.2). A third-generation gravitational wave detector called the Einstein Telescope (ET) (Punturo 2010) is also under design study, and would offer another order of magnitude increase in sensitivity. This would bring hundreds of currently known pulsars into the range where we could beat spin-down limits (see Section 2.3), and also may coincide with the completion of the Square Kilometre Array (SKA) radio telescope, which may give us a vastly larger number of sources to target. Estimates suggest the SKA may detect over half of the observable pulsars within the galaxy giving ∼20 000 potential sources (Cordes et al. 2004) with ∼1000 of them being millisecond pulsars and some of which could have large spin-down luminosities. Design strain curves for aLIGO, AdvVirgo and the ET in two different potential configurations are shown in Fig. 1.

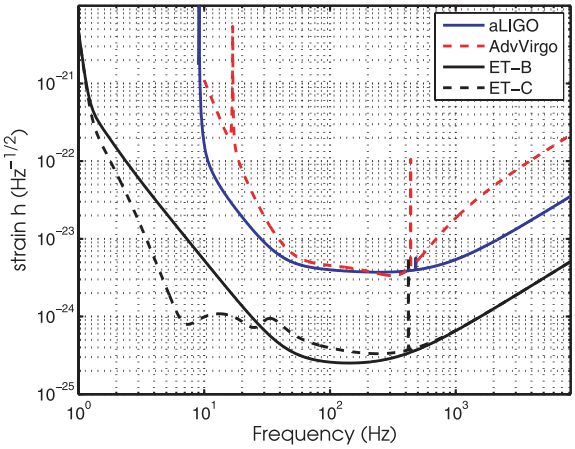

Figure 1. Design strain curves for aLIGO (LIGO Scientific Collaboration 2009) (using the zero detuning, high laser power configuration), AdvVirgo (the baseline sensitivity used here is that of 2009 May 12 found at http://wwwcascina.virgo.infn.it/advirgo/), and the ET in both ET-B and ET-C configurations (taken from http://www.et-gw.eu/etsensitivities).

Assuming that the star is emitting at its spin-down limit, and that a fully coherent search can be performed, we have estimated the angle averaged S/N for all known pulsars for which a spin-down limit can be calculated[2] given 1 yr observation times for joint aLIGO and AdvVirgo observations (ALV) and for the ET in two potential configurations – ET-B and ET-C (see Section 2.3).

For the Crab pulsar we will estimate the S/N using a limit based on the observed upper limit, which at $h_0^{95\,\mathrm{per\,cent}} = 2.0 \times 10^{-25}$ (Abbott et al. 2010) is approximately seven times below the spin-down limit of 1.4×10^{-24} for a star with the canonical moment of inertia and a distance of 2 kpc. This result also beats limits of Palomba (2000) based on the Crab pulsar's observed braking index. For the Vela pulsar and B0540−69 (J0540−6919), for which braking indices can also be reliably measured, we use upper limit estimates based on those calculated by Palomba (2000). For Vela (using the Vela age of 11 000 yr given in Abadie et al. 2011) this gives limits four times lower than the spin-down limit of 3.3×10^{-24}, and for B0540−69 this gives a limit six times lower than the spin-down limit of 5.2×10^{-26}. For these three pulsars our S/N estimates used known values of the pulsar inclination angle and gravitational wave polarization angles as taken from fits to the pulsar wind nebulae in Ng & Romani (2008). As can be seen in Fig. 3 these three pulsars would have S/N greater than 5 for all future detectors if emitting at their spin-down, or observationally constrained, upper limits. They are not included in the numbers quoted in the rest of this section.

2.1 Assessing detection and parameter estimation

We can estimate the S/N for all known pulsars for a given gravitational wave detector, or a set of detectors, to assess our ability to detect them and perform parameter estimation. The S/N, ρ, can be calculated from the square root of the inner product of the signal h with itself, $\rho = \sqrt{(h|h)}$, (the inner, or scalar, product for real time domain functions is given by $(x|y) = (2/S_n(\nu))\int_0^T x(t)y(t)\mathrm{d}t$) which

[2] Many of the millisecond pulsars found so far are seen in GCs, and accelerations within these clusters can mask the spin-down and even produce an observed spin-up, so in this section we exclude these.

given the time domain signal model of (e.g. Dupuis & Woan 2005)

$$h(t) = h_0\left[\tfrac{1}{2}(1+\cos^2\iota)F_+(t,\psi)\cos\phi(t) + \cos\iota F_\times(t,\psi)\sin\phi(t)\right] \quad (1)$$

gives

$$\rho = \left[\frac{h_0^2}{S_n(\nu)}\frac{T}{N}\sum_k^N\left(\left[\frac{1}{2}(1+\cos^2\iota)F_+(t_k,\psi)\right]^2 + [\cos\iota F_\times(t_k,\psi)]^2\right)\right]^{1/2}, \quad (2)$$

under the assumption that $\nu T \gg 1$, and where $S_n(\nu)$ is the frequency-dependent one-sided noise power spectral density[3] in Hz, T is the total observation time in seconds, N is the number of samples used, and F_+ and $F_\times$ are the source position and polarization-dependent detector antenna patterns (see e.g. Jaranowski, Królak & Schutz 1998).

The S/N depends on the orientation of the pulsar, so upper and lower values can be set for the best and worst case orientations. The best case in terms of S/N is for a pulsar's spin axis to be along the line of sight ($\iota = 0^\circ$ or 180°, or $\cos\iota = \pm 1$), which gives rise to circularly polarized radiation; the worst case is for the pulsar's spin axis to perpendicular to the line of site ($\iota = 90^\circ$ or $\cos\iota = 0$), which gives rise to just linearly polarized radiation. The S/N ranges over a factor of ∼3 between best and worst cases, and the angle averaged, or expected, S/N (averaging over a uniform distribution in $\cos\iota$, ψ and ϕ_0) is ∼1.69 times below that for best case orientation value. For a fixed S/N the angle averaged value of h_0 is 1.89 times the value needed to give the same S/N for the best case orientation[4] (i.e. for the best case orientation a smaller value of h_0 will produce an equivalent S/N). In this section, we will be asking the question 'given that the star is emitting gravitational waves at an amplitude X, what is the expected S/N it would have?', whereas in Section 4 we will be asking the question 'given that the signal has an S/N of X, what will the expected h_0 (or parameter such as ratio to spin-down limit or mass quadrupole that scales with h_0) be?'. When estimating the number of pulsars that are potentially observable using either an expected S/N calculated from a given h_0 or an expected h_0 calculated from a given S/N, the results will be slightly different.

2.1.1 *Detection statistic*

For the rest of this paper we will assume an S/N for a signal that we believe provides a good chance of detection. To do this we will use Bayesian hypothesis testing to provide a detection statistic with which to assess detection efficiency at different S/N (see e.g. Clark et al. 2007 or Prix & Krishnan 2009). We produced a Bayes factor in which the two competing models are that of data containing Gaussian noise *and* a known pulsar signal compared to data just containing Gaussian noise. Uniform priors were set for the signal parameters, and a prior odds for the competing models of 1 was used. To assess this we produced Monte Carlo simulations of 2000 signals, with fixed sky position, but randomly chosen values of $\cos\iota$, ψ and ϕ_0, in different realizations of noise at a range of S/N. The approach is essentially using what is described as the $\mathcal{B}$-statistic in Prix & Krishnan (2009), which they show to be slightly more efficient, although computationally more expensive, than the more widely used $\mathcal{F}$-statistic (Jaranowski et al. 1998; Abbott et al. 2004b).

If we have a threshold false alarm rate due to background of 1 per cent, then Monte Carlo simulations show that an S/N of 5 gives a detection probability of 95 per cent (see Fig. 2) which we will use as our required value for confident detection in the subsequent sections. Real data are generally non-stationary and may contain interference, so this idealized detection statistic may be slightly optimistic, but should be close to reality, given well-understood and cleaned data.

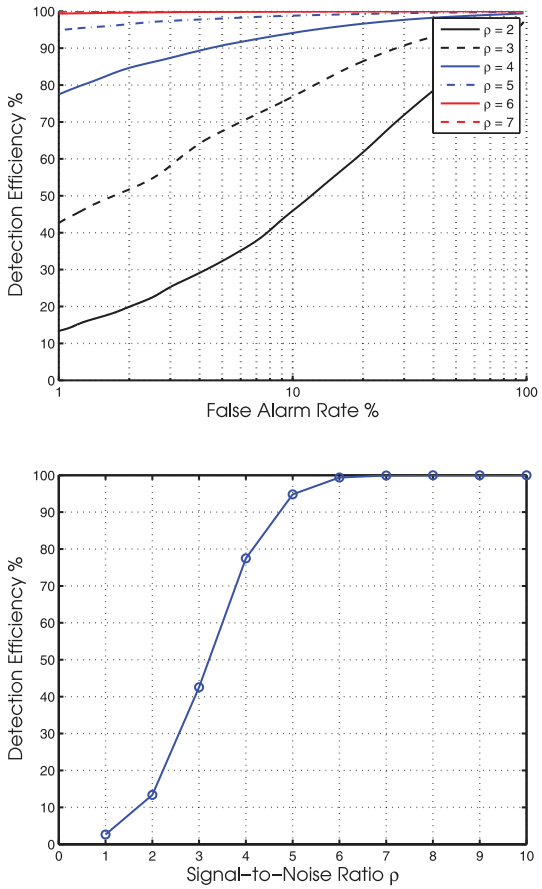

Figure 2. The top figure shows the Receiver Operating Characteristic (ROC) curves for a variety of S/N (ρ), with the $\rho = 4$ curve showing the same form as that given by Prix & Krishnan (2009). The bottom figure shows the detection efficiency of the known pulsar search as a function of S/N given a background false alarm rate of 1 per cent.

2.2 Second-generation detectors

For aLIGO we assume two 4 km interferometers based at the Hanford site and one 4 km interferometer at the Livingston site all with equivalent sensitivity and operating at the designed value (LIGO

[3] This is related to the noise variance via $S_n = 2\sigma^2\Delta t$, where Δt is the sample interval in the data time series.

[4] Note that the angle averaged S/N for a given value of h_0 and the angle averaged h_0 for a given S/N are not interchangeable. This comes about because for the first case the angle averaged S/N $\langle\rho\rangle \propto h_0\langle C\rangle$, whereas in the second case the angle averaged amplitude $\langle h_0\rangle \propto \rho\langle 1/C\rangle$, where $C = \sum_k^N([\frac{1}{2}(1+\cos^2\iota)F_+(t_k,\psi)]^2 + [\cos\iota F_\times(t_k,\psi)]^2)^{-1/2}$ and $\langle f(y)\rangle = \int_{y\min}^{y\max} p(y)f(y)\,\mathrm{d}y$. For an individual pulsar, i.e. a single sky position, the dependence on polarization angle disappears for data spans a lot greater than a day, and as can be seen from equation (2) the phase dependence is no longer present, so the orientation angle is the only one needing averaged over for which we use a uniform distribution between −1 and 1 giving $p(\cos\iota) = 1/2$.

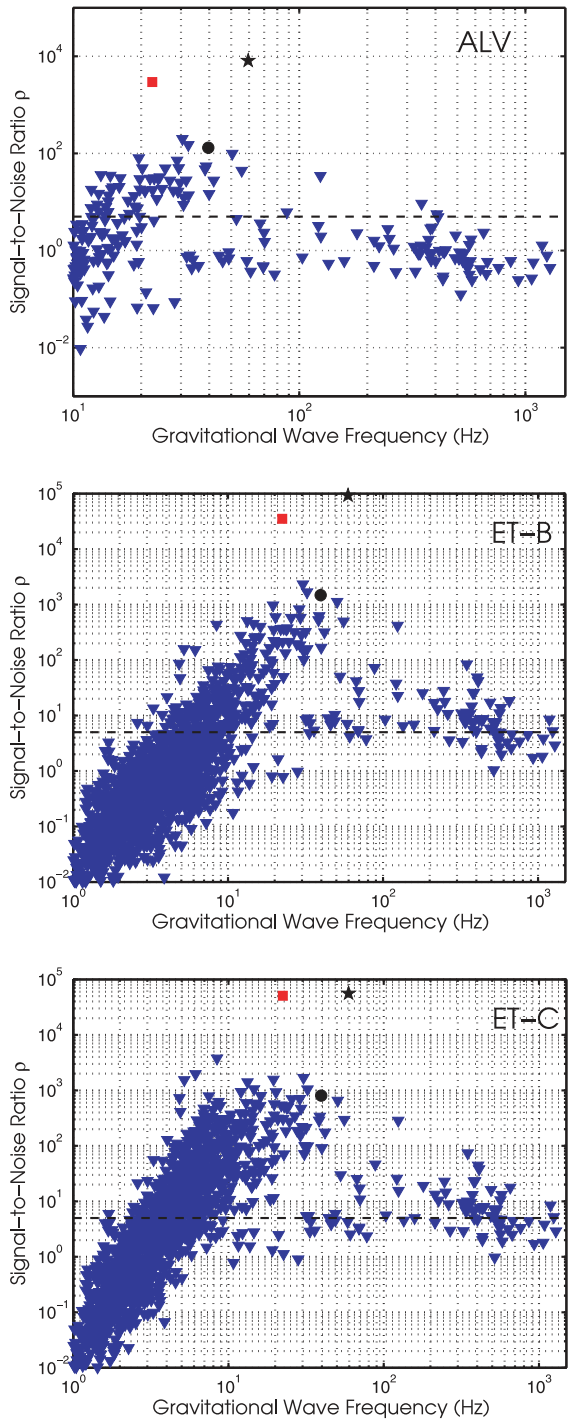

Figure 3. The angle averaged S/N for all currently known non-GC pulsars with measured spin-down values expected for ALV (upper panel) and the ET in ET-B (middle panel) and ET-C (bottom panel) configurations assuming emission at the spin-down limit (see text for exceptions). The ⋆ represents the value for the Crab pulsar, the • represents the value for B0540−69 and the ■ represents the value for the Vela pulsar. The thick horizontal dashed line shows an S/N of 5.

Scientific Collaboration 2009). For AdvVirgo we use one 3 km interferometer at its design sensitivity (see Fig. 1). Fig. 3 gives the angle averaged S/N for 1 yr of observations with all these detectors (three aLIGO and one AdvVirgo, or ALV from now on) and shows that potentially 58 pulsars could be observed with an S/N greater than 5 (best case orientation gives 74 with S/N above 5 and the worst case orientation gives 47 with S/N above 5). Some similar, but unpublished work, has been presented by Santostasi (2006).

2.3 Third-generation detectors

Some assessment of detectability of the currently known pulsars, based on their spin-down limits, has previously been performed for the proposed third-generation detector called the ET in Andersson et al. (2011) (along with the potential for observing neutron stars through other gravitational wave emission mechanisms), although this was just for the ET-B configuration (see below). Here, as above, we will calculate S/N for the ET. In Fig. 3 we show S/N based on the sensitivity of the ET-B configuration, as described in Hild, Chelkowski & Freise (2008), with three interferometers on one site (given here as the current Virgo site) in an equilateral triangle configuration (Freise et al. 2009). For this configuration of ET-B we could potentially see 312 pulsars with an angle averaged S/N greater than 5 (or 405 for the best case and 223 for worst case). A 'xylophone' configuration (ET-C) consisting of different detectors optimized for different frequency bands, with comparable high-frequency sensitivity, but better low-frequency sensitivity than ET-B, has also been proposed (Freise et al. 2009; Hild et al. 2010). In Fig. 3, we show the S/N based on the ET-C sensitivity (again with the same layout as ET-B). For ET-C we could potentially see 648 pulsars with an orientation angle averaged S/N greater than 5 (or 771 for the best case and 528 for worst case). These numbers are around double those for the ET-B configuration due to the lower frequency sensitivity increase, suggesting that this may be the preferred configuration for known pulsar searches. However, we should be cautious as we will see in Section 4 (and also as stated in Andersson et al. 2011) that many of these will have to be rather exotic, and therefore probably less realistic, stars to be seen at these levels. A further configuration, called ET-D (Hild et al. 2011), is now also available, although it is very comparable to ET-C for a wide range of frequencies, so we have not used it in these studies.

2.4 Parameter estimation

Our ability to constrain the physical parameters of a source is obviously dependent on the S/N, but the correlated physical parameters we use to describe the signal can mean that rather unintuitively a higher S/N signal may not give the best constraints on h_0.

We have simulated a selection of pulsars that give best case and worst case S/N of around 5, 10, 50 and 100 for ALV (as shown in Fig. 3) to assess the level of uncertainty on estimates of their parameters assuming they are observable at that level. To do this we used the Markov chain Monte Carlo technique described in Abbott et al. (2010) to produce posterior probability density functions (PDFs) on the four parameters defined in Section 1. Uncertainties on parameters can be assessed using a Fisher Information Matrix approach, for example as done by Jaranowski & Królak (2010), but as they show, such a method will give *biased* error estimates overestimating the uncertainty for signals near $\cos\iota = \pm 1$, even for very strong signals with S/N approaching 1000.

We calculate the appropriate signal strength needed to give S/N of 5, 10, 50 and 100 for both the best and worst case orientations (see Table 1) and produce PDFs on many realizations of the data to give an average PDF. These can be seen in Fig. 4 and the mean parameter values (not the peak in the posterior) and their 1σ uncertainties obtained from the PDFs are given in Table 1. Examples of pulsars that if emitting at their spin-down limits might be

Table 1. Mean parameter estimates, and their uncertainties, at a variety of S/N given best and worst case orientations. The true value of h_0 is given followed by the average (over many trials) mean estimate and standard deviation on each parameter. The fractional uncertainty on h_0 is also given. In the low S/N cases where the signal peaks near zero a 95 per cent confidence upper limit is given. The true values of ϕ_0 and ψ in all cases are $\pi$and 0 rad, respectively. The parameter estimates have been performed assuming the ALV combination at design sensitivity.

	True h_0	ρ	$\overline{h_0} \pm \sigma_{h_0}$	$\sigma_{h_0}/\overline{h_0}$ (per cent)	$\overline{\phi_0} \pm \sigma_{\phi_0}$	$\overline{\cos\iota} \pm \sigma_{\cos\iota}$	$\overline{\psi} \pm \sigma_{\psi}$
$\cos\iota = 0$	5.24×10^{-27}	1.7	$h_0^{95\,\text{per cent}} = 1.08 \times 10^{-26}$	*	3.28 ± 1.24	-0.02 ± 0.46	0.00 ± 0.40
$\cos\iota = 1$	5.24×10^{-27}	5.0	$9.27 \pm 3.72 \times 10^{-27}$	40	3.21	0.51 ± 0.26	*
$\cos\iota = 0$	1.59×10^{-26}	5.0	$1.49 \pm 0.62 \times 10^{-26}$	42	3.20 ± 0.44	0.00 ± 0.29	0.03 ± 0.21
$\cos\iota = 1$	1.59×10^{-26}	15.1	$2.27 \pm 0.55 \times 10^{-26}$	24	3.19	0.67 ± 0.18	*
$\cos\iota = 0$	5.96×10^{-27}	3.4	$h_0^{95\,\text{per cent}} = 9.15 \times 10^{-27}$	*	3.12 ± 0.90	0.16 ± 0.36	-0.02 ± 0.33
$\cos\iota = 1$	5.96×10^{-27}	10.0	$8.98 \pm 2.49 \times 10^{-27}$	28	3.06	0.64 ± 0.21	*
$\cos\iota = 0$	1.77×10^{-26}	10.0	$1.76 \pm 0.27 \times 10^{-26}$	15	3.17 ± 0.14	-0.01 ± 0.06	0.01 ± 0.07
$\cos\iota = 1$	1.77×10^{-26}	29.6	$2.24 \pm 0.36 \times 10^{-26}$	16	3.15	0.78 ± 0.14	*
$\cos\iota = 0$	2.58×10^{-26}	17.7	$2.60 \pm 0.22 \times 10^{-26}$	8	3.12 ± 0.08	0.00 ± 0.04	0.01 ± 0.04
$\cos\iota = 1$	2.58×10^{-26}	50.0	$3.10 \pm 0.40 \times 10^{-26}$	13	3.19	0.82 ± 0.11	*
$\cos\iota = 0$	7.31×10^{-26}	50.0	$7.30 \pm 0.19 \times 10^{-26}$	3	3.14 ± 0.03	0.00 ± 0.01	0.00 ± 0.02
$\cos\iota = 1$	7.31×10^{-26}	141.5	$8.40 \pm 0.73 \times 10^{-26}$	9	3.26	0.87 ± 0.08	*
$\cos\iota = 0$	7.40×10^{-26}	33.8	$7.39 \pm 0.33 \times 10^{-26}$	4	3.15 ± 0.04	0.00 ± 0.02	0.00 ± 0.02
$\cos\iota = 1$	7.40×10^{-26}	100.0	$8.41 \pm 0.74 \times 10^{-26}$	9	3.14	0.88 ± 0.08	*
$\cos\iota = 0$	2.18×10^{-25}	100.0	$2.18 \pm 0.03 \times 10^{-25}$	1	3.14 ± 0.01	0.00 ± 0.01	0.00 ± 0.01
$\cos\iota = 1$	2.18×10^{-25}	294.8	$2.37 \pm 0.12 \times 10^{-25}$	5	3.12	0.92 ± 0.05	*

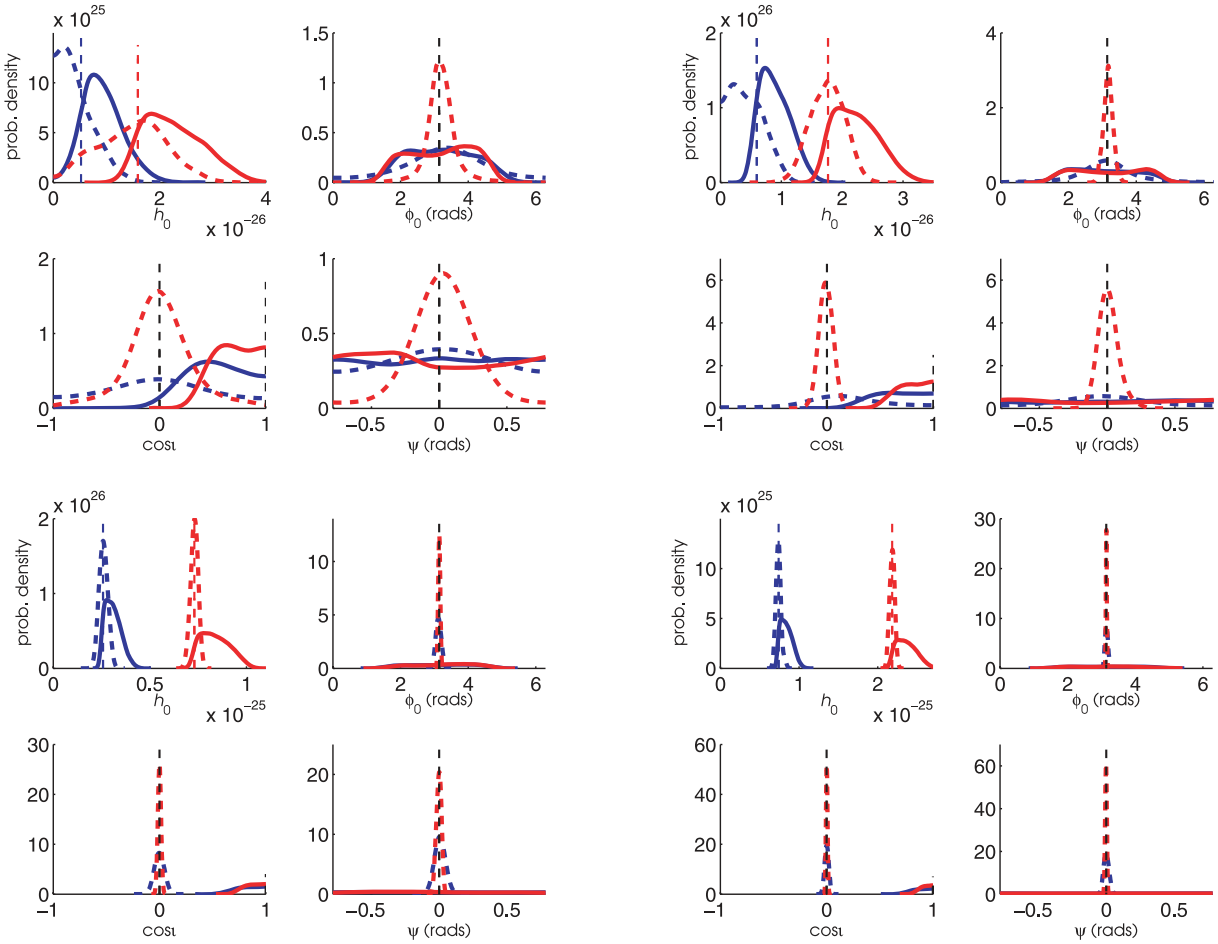

Figure 4. Each panel shows the average posterior probability density functions on the four gravitational wave signal parameters of h_0, ϕ_0, $\cos\iota$ and ψ for four simulated signals. The four signals in each panel (from top left to bottom right) correspond to the parameters given in each of the four sections (from top to bottom) of Table 1. In an individual panel lines of the same colour represent signals with identical amplitude; solid lines represent the signals with the worst case orientation ($\cos\iota = 0$) and dashed lines represent the signals with the best case orientation ($\cos\iota = 1$). The tapering off of the ϕ_0 posteriors for the best case orientation at $\pi \pm \pi/2$ is an artefact of the plotting and these parameters should really have abrupt cut-offs at these values.

observed with ALV at S/N of ∼5, 10, 50 and 100 are, respectively, J1959+2048, J0737−3039A (the millisecond pulsar in the famous double pulsar system), J0537−6910 (an interesting young pulsar in the Large Magellanic Cloud, with a high glitch rate and large spin-down rate) and J1952+3252. The main results of Table 1, i.e. the relative uncertainties in h_0 for different S/N signals given the best and worst case orientation scenarios, are extrapolated to higher S/N and shown as the thick black lines in Fig. 8 (they are equivalent to the uncertainties on the quadrupole assuming the distance is precisely known).

It can clearly be seen by looking at equation (1), and from our posteriors in Fig. 4, that for a signal with $\cos\iota \approx \pm 1$ the h_0 and $\cos\iota$ parameter are highly correlated, which leads to the h_0 posterior being spread to higher values, and $\cos\iota$ extending towards zero. In such a case the ϕ_0 and ψ parameters are also very highly correlated, with the posterior on ψ being flat over its range (see Fig. 4), and ϕ_0 only constrainable to within a 180° range, i.e. the direction the star is rotating in can be found, but otherwise these parameters are ill defined to represent such a situation. These correlations can be seen more easily in Fig. 5, and they lead to the slightly paradoxical fact that when comparing equivalent signals in Fig. 4 we can actually place the tightest constraints on h_0 for the worst case orientation, i.e. lower S/N, signals! Due to these correlations we do not quote mean, or uncertainty, values on ψ in Table 1 as they are meaningless; we also only quote mean values for ϕ_0 to show that the value found is oriented in the correct sense. If we were to cast the uncertainties in ι and ψ as a solid angle then at $\cos\iota = \pm 1$ the associated error ellipses for different S/N would be entirely proportional to the error on ι alone (i.e. the error on ψ stays constant). For a signal with S/N ≈ 20 the best and worst case solid angles covering the $\sim 1\sigma$ probability contour in $\iota - \psi$ space are 0.35 sr and 6×10^{-4} sr, respectively. The ratio of these areas scales very roughly linearly with S/N (within about a factor of 2) as 50ρ, up to S/N of ∼100.

In the case of pulsars like the Crab pulsar where X-ray observations and modelling of their pulsar wind nebulae are possible, there is additional information placing tight constraints on the orientation and polarization angles. Including this will break the degeneracies between parameters, for example as performed in the search by Abbott et al. (2008a). In Fig. 6, the fractional uncertainty on the

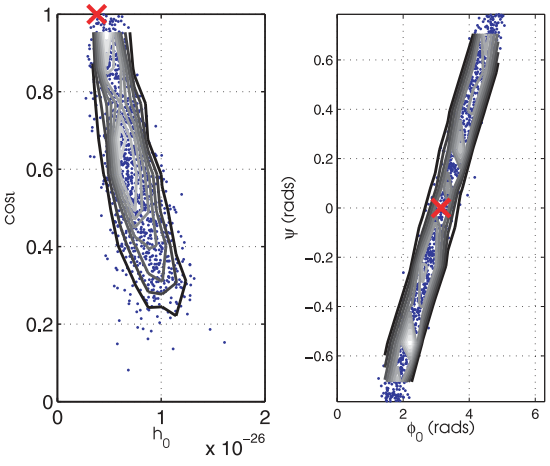

Figure 5. The correlations between the h_0 and $\cos\iota$, and ϕ_0 and ψ parameters for a simulated signal with the best case orientation. The data points from the Markov Chain Monte-Carlo (MCMC) and the probability contours derived from them are shown. The cross marks the parameters used to produce the signal.

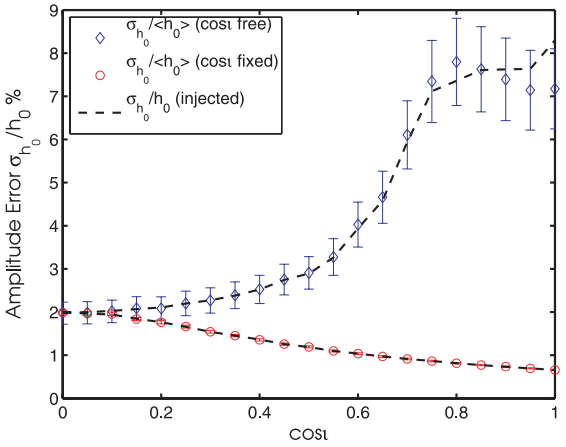

Figure 6. The fractional uncertainties on amplitude (standard deviation over mean $-\sigma_{h_0}/\overline{h_0}$) from many simulations of performing parameter estimation on a signal (with an S/N of 50 calculated for the worst case orientation) when all parameters are unknown (blue) compared to when the $\cos\iota$ and ψ parameters are known and fixed in the search. Also shown as dashed lines are the fractional uncertainties given the actual signal h_0 values rather than the mean recovered value.

amplitude estimate (averaged over many simulations) is shown as a function of $\cos\iota$ for simulated sources where in one case the orientation and polarization angles are known (i.e. these are fixed at their known values and not searched over, equivalent to having very tight prior distributions on these parameters), and in the other case that they are unknown (i.e. the whole range of $\cos\iota$ and ψ has to be searched over with uniform priors). It can be seen in Fig. 6 that for the case where all parameters are searched over the fractional uncertainty on the amplitude increases with $\cos\iota$, with the steepest rise between about $\cos\iota = 0.5$ and 0.7. However, when $\cos\iota = 0.8$ the fractional error slightly decreases again suggesting that a $\cos\iota = \pm 1$ does not actually given the worst estimate of h_0. This is actually slightly misleading as the reason for the downturn becomes more apparent from looking at the curves of fractional uncertainty given the true h_0 values (rather than the fractional uncertainty based on the mean h_0 value), and plots of PDFs for h_0 in Fig. 4 – at values of $\cos\iota$ approaching ± 1 the mean estimate of h_0 starts to increase relative to the true value, whilst the uncertainty starts to plateau, leading to the downturn. This means that estimates of h_0 when $\cos\iota = \pm 1$ would still give values furthest from the true value, but due to the shifting of the whole posterior towards higher values rather than it widening. For the case where the $\cos\iota$ and ψ values are held fixed at their known values during the parameter estimation the fractional amplitude uncertainty behaves as one would expect and decreases as the S/N increases as $\cos\iota$ tends to 1. The fractional amplitude uncertainty, whether calculated with the mean or true h_0 value, follows the same path, because the posterior stays symmetrical about the true value.

Current detectors have systematic uncertainties in amplitude and phase due to calibration in the region of 10–15 per cent and 5°, respectively (Abadie et al. 2010). For second-generation detectors it is hoped to further reduce amplitude uncertainty to less than 10 per cent, but if we are lucky enough to see any high S/N ($\gtrsim 20$) signals this may be the main source of error in the h_0 estimates.

2.4.1 *Dependence on distance*

The gravitational wave amplitude, and its uncertainties, can be directly measured. However, if we want to convert this into a physical

Table 2. The uncertainties on the quadrupole moment at a variety of S/N given best and worst case orientations with uncertainties on the distance measurement of $\sigma_r = 1$, 5, 10, 20 and 50 per cent.

			$\sigma_{Q_{22}}/\overline{Q_{22}}$ (per cent)				
	ρ	$\sigma_{h_0}/\overline{h_0}$ (per cent) or $\sigma_r = 0$ per cent	$\sigma_r = 1$ per cent	$\sigma_r = 5$ per cent	$\sigma_r = 10$ per cent	$\sigma_r = 20$ per cent	$\sigma_r = 50$ per cent
$\cos\iota = 0$	1.7	*	*	*	*	*	*
$\cos\iota = 1$	5.0	40	41	40	43	46	59
$\cos\iota = 0$	5.0	42	42	44	45	49	60
$\cos\iota = 1$	15.1	24	25	25	27	32	44
$\cos\iota = 0$	3.4	*	*	*	*	*	*
$\cos\iota = 1$	10.0	28	29	29	30	35	50
$\cos\iota = 0$	10.0	15	16	17	19	25	38
$\cos\iota = 1$	29.6	16	17	17	20	26	41
$\cos\iota = 0$	17.7	8	9	10	13	21	40
$\cos\iota = 1$	50.0	13	13	14	17	23	40
$\cos\iota = 0$	50.0	3	3	6	11	19	36
$\cos\iota = 1$	141.5	9	9	10	13	21	38
$\cos\iota = 0$	33.8	4	5	7	11	19	36
$\cos\iota = 1$	100.0	9	9	10	13	20	39
$\cos\iota = 0$	100.0	1	2	5	10	18	36
$\cos\iota = 1$	294.8	5	6	7	11	20	39

quantity related to the star, such as the mass quadrupole moment (see equation 3), then the uncertainty on the distance to the pulsar will come into play. Current distance measurements for nearby pulsars come from parallax measurements, but for most others come from dispersion measure observations extrapolated from a model of the Galactic free electron distribution (Cordes & Lazio 2002). For the majority of pulsars distances generally have uncertainties at $\sim$20 per cent or more (even $>$100 per cent) of the best-fitting values. In the future, with instruments like the SKA, direct parallax measurements may push these errors down to the level of $<$20 per cent for many millisecond pulsars out to 9 kpc (Smits et al. 2011). Here we will look at how different distance uncertainties affect estimates of the quadrupole moment for a variety of S/N and for the best and worst orientations.

It can be seen from Table 2 and Fig. 7 that for the lowest S/N signals distance errors of 10–20 per cent give only a relatively small increase in the uncertainty with which the quadrupole moment can be measured. The convergence of the uncertainties on the measurement for the best and worst case orientations, i.e. when the uncertainties become dominated by the distance uncertainty rather than that on the measurement, can be seen in Fig. 8. For strong signals (S/N $\gtrsim$ 50) the uncertainty on distance will start to dominate quadrupole estimates if it is $\gtrsim$10 per cent and will also swamp any differences due to orientation.

Seto (2005) suggests that gravitational wave observations of pulsars could be used to determine their distances to $\lesssim$10 per cent, but only for nearby stars ($\lesssim$100 pc) with very large S/N and high frequencies. This is therefore unlikely to help constrain distances better than other techniques for the vast majority of known pulsars.

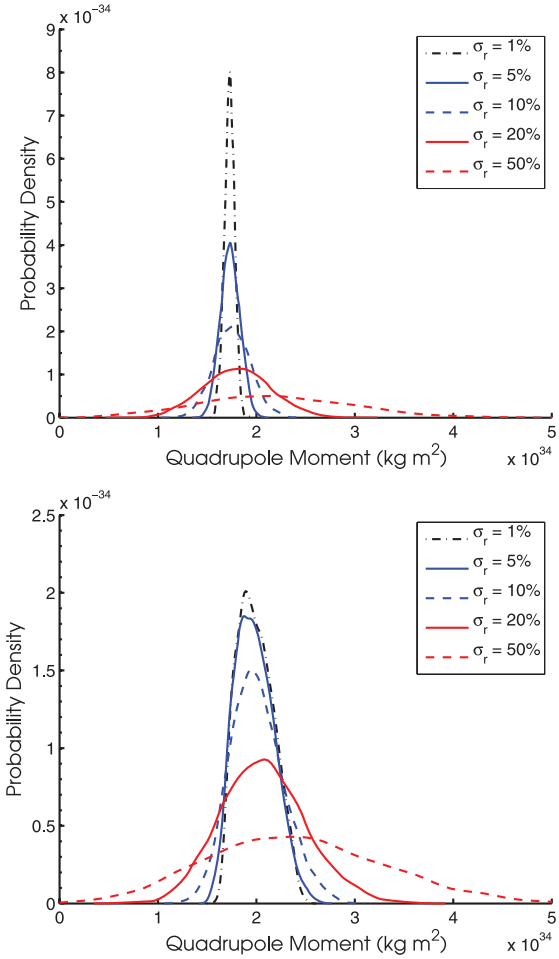

Figure 7. The PDF for the quadrupole moment, Q_{22}, given a simulated signal for the pulsar with $h_0 = 7.31 \times 10^{-26}$ in Table 1 at both $\cos\iota = 0$ (top plot) and $\cos\iota = 1$ (bottom plot), with S/N of 50 and 141.5, respectively, over a range of distance uncertainties, σ_r, of 1, 5, 10, 20 and 50 per cent.

3 EQUATIONS OF STATE

As discussed in Lattimer & Prakash (2007) there are many ways to attempt to observationally constrain the EoS of a neutron star through inferences about their mass and radius, e.g. via various observations of binary and accreting systems. Observations of gravitational waves from merging neutron stars (or merging neutron stars and black holes) can also give mass and radius measurements, and

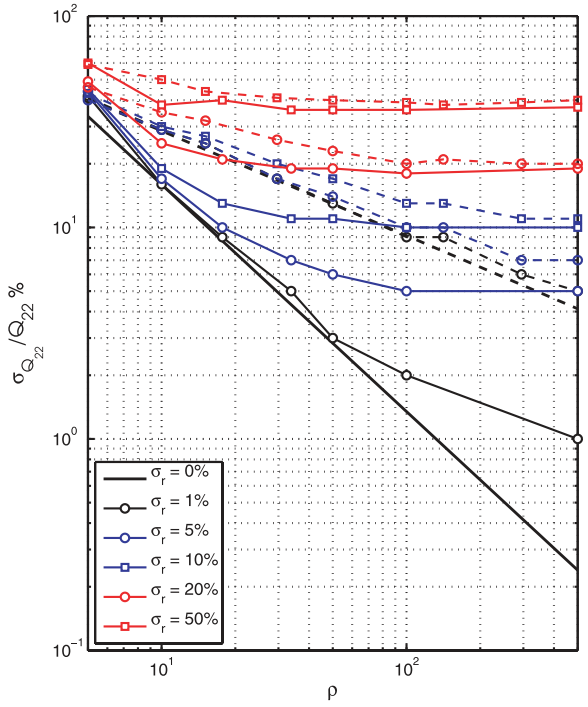

Figure 8. The uncertainties on the estimate of Q_{22} given in Table 2 for a variety of distance uncertainties and the best (dashed lines) and worst (solid lines) case orientations.

information about the EoS properties from tidal effects during the inspiral (Flanagan & Hinderer 2008) and the point at which the star breaks up (Andersson et al. 2011).

However, emission of gravitational waves from individual neutron stars, either through a continuous emission from a sustained triaxiality or through short bursts from vibrational modes (e.g. Andersson & Kokkotas 1998), could also provide constraints. Due to the low amplitude of gravitational waves expected from these sources, such observations would most likely only be available for Galactic sources. Rather than explicitly studying what observations of continuous gravitational waves from a triaxial neutron star can tell us about the stars EoS, we flip the question and look at the maximum magnitudes of signals we could possibly expect for a variety of EoS. The maximum values we discuss are likely to be at the extreme end of possibility and in reality they could be overestimated (or possibly, but less likely, underestimated) by several orders of magnitude due to the uncertain physics of these objects.

3.1 Quadrupole moments

The observable in known pulsar searches that relates to the neutron star EoS is the gravitational wave amplitude h_0. This is directly related to the star's $l = m = 2$ mass quadrupole moment via

$$Q_{22} = h_0 \left(\frac{c^4 r}{16\pi^2 G \nu^2} \right) \sqrt{15/8\pi}, \tag{3}$$

where r is the distance in m and ν is the rotation frequency in Hz. The quadrupole moment is often parametrized in terms of the star's principal moment of inertia, I_{zz}, and ellipticity, ε, via $\varepsilon I_{zz} = \sqrt{8\pi/15} Q_{22}$ (Owen 2005). However, these two parameters cannot be disentangled from observations, although the range of moments of inertia can be implied from various theoretical EoS mass and radius relations (generally thought to be in the range 1–3×10^{38} kg m^2; e.g. Abbott et al. 2007a), allowing ellipticities to be implied from observations. Often in gravitational wave literature results are cast in terms of ellipticity as it feels a more physically tangible parameter, giving a physical 'size' of the distortion of a star.

Following, for example, Ushomirsky, Cutler & Bildsten (2000) and Owen (2005) the quadrupole for an incompressible star with a thin curst can be written as

$$Q_{22} = \frac{\gamma \mu R^6 \langle \sigma_{22} \rangle}{GM}, \tag{4}$$

where $\langle \sigma_{22} \rangle$ is the weighted average strain on the crust (contributing to the 22-quadrupole), R and M are the star's radius and mass, and $\gamma \approx 13$. Often, this equation is quoted as an upper limit on Q_{22} by inserting the maximum breaking strain $\sigma_{\max}$; however as noted in Ushomirsky et al. (2000) the equation is equally applicable to providing an estimate of the crustal strain. The parameter in equation (4) that is most dependent on the detailed make-up of the star is the shear modulus μ, which between theories can potentially vary by many orders of magnitude. Below we will make the assumption that the stars are incompressible and therefore use equation (4) in calculations, along with an assumed $\gamma = 13$ (for a conventional neutron star γ can be related to the ratio of the thickness of the star's crust, ΔR, to its radius via $\gamma \approx 120 \Delta R/R$). It should also be noted that these assume the Cowling approximation and neglect self-gravity of the density perturbations. Ushomirsky et al. (2000) showed that including self-gravity can increase the quadrupole calculations by between 25 and 200 per cent, and similarly Haskell, Jones & Andersson (2006) found that self-gravity can affect results by factors of between 0.5 and 3.

For the millisecond recycled pulsars spin-down arguments alone tell us that their quadrupoles must be relatively small ($\lesssim 10^{30}$ kg m^2). Such a quadrupole would be obtainable with any EoS (see below) meaning that if detected they are not helpful in differentiating between theories, although multiple detections could build up useful statistics on their properties and limits on their internal magnetic fields.

Here, we will review some of the work presented by Owen (2005) regarding maximum sustainable quadrupoles for a variety of stellar EoS.

3.1.1 *Normal neutron stars*

For stars made from *normal* neutron star matter (neutrons, protons and electrons) Ushomirsky et al. (2000) provide a detailed model of the quadrupole (see equation 69). Owen (2005) applies standard numbers in this definition (and corrects the definition of the shear modulus to be 4×10^{29} erg cm^{-3}, or 2.5×10^{-4} MeV fm^{-3}) to give

$$Q_{22} = 2.4 \times 10^{32} \text{ kg m}^2 \langle \sigma_{0.1} \rangle R_{10}^{6.26} M_{1.4}^{-1.2}, \tag{5}$$

where $\langle \sigma_{0.1} \rangle$ is an averaged strain of 0.1, R_{10} is the radius in units of 10 km, and $M_{1.4}$ is the mass in units of 1.4 $M_\odot$. Uncertainties in the star's mass will only affect this estimate by small amounts e.g. given theoretical[5] and observational bounds on the mass between

[5] Theoretically, the lower bound on neutron star mass could be as small as $\sim 0.1\,M_\odot$ (Lattimer & Prakash 2001), but we will assume our population of known pulsars is similar to the ones with observed masses (see e.g. fig. 3 of Lattimer & Prakash (2007), or the figure maintained at http://www.stellarcollapse.org/nsmasses). A discussion of gravitational waves from neutron stars at the lowest end of the possible mass range can be found in Horowitz (2010), which suggest these are potentially strong sources, but it is very unlikely that any known pulsar would be of this type.

$\sim$1 and 2.5 $M_\odot$ the quadrupole will only vary within about a factor of 3 from 0.5 to 1.5. However, for the radius, with its far larger exponent, small differences can give a larger range of possible quadrupoles. If we take a theoretical range from 10 to 15 km then this can change the quadrupole by about an order of magnitude. The most massive stars will also have the smallest radii, so from this we get an uncertainty range on the quadrupole from the unknown mass and radius of between $\sim$0.5 and 20 times the value in equation (5), with the most massive, but smallest stars at the lower end and vice versa.

Here, we will assume the breaking strain is at the maximum value of $\sigma_{\max} \approx 0.1$ calculated by Horowitz & Kadau (2009) (much previous work has assumed a maximum breaking strain of $10^{-5} \leq \sigma_{\max} \leq 10^{-2}$). This value of the breaking strain was calculated for normal neutron star matter, but for other situations it may well not be a valid assumption. Using the higher value from the mass/radius uncertainty as an upper limit, and inserting in the maximum breaking strain, we *could* get normal neutron stars with quadrupoles of $Q_{\max} \approx 4.5 \times 10^{33}\,\mathrm{kg\,m^2}$. Converting this to an approximate (order of magnitude) estimate of the ellipticity, assuming the canonical moment of inertia, would give $\varepsilon \approx 6 \times 10^{-5}$. Although the reasoning behind it is quite different [i.e. just coming from plugging in masses and radii at the extent of their ranges, with the majority of the increase over the fiducial value in Owen (2005) coming from using a maximum radius of 15 km] this value is very similar to that produced by the perturbative approach to the problem performed by Haskell et al. (2006). Assuming the maximum breaking strain of 0.1 they would produce a maximum quadrupole (see table 4 of Haskell et al. 2006) of $Q_{\max} = 3.1 \times 10^{33}\,\mathrm{kg\,m^2}$ for a star with a mass of 1.4 $M_\odot$, radius 12.3 km and crust thickness 1.5 km.

3.1.2 Hybrid crystalline colour-superconducting star

In Knippel & Sedrakian (2009), Haskell et al. (2007) and Lin (2007) the quadrupole is calculated for crystalline colour-superconducting (CSS) hybrid stars. In these stars the gravitational wave emission mainly comes from a deformed interior core of quark matter. The quadrupole can again be approximated by equation (4), but with a shear modulus given by (Mannarelli, Rajagopal & Sharma 2007)

$$\mu = 2.47\,\mathrm{MeV\,fm^{-3}}\,\Delta_{10}^2 \mu_{q400}^2, \tag{6}$$

where Δ_{10} is the gap parameter in units of 10 MeV, and μ_{q400} is the quark chemical potential in units of 400 MeV (which in Mannarelli et al. 2007 is estimated to be in the range $350 \leq \mu_q \leq 500$ MeV), and the stellar mass and radius are replaced by those of the quark core. Knippel & Sedrakian (2009) assume a range of gap parameters[6] $10 \leq \Delta \leq 50$ MeV, and find a maximum core mass of 0.8 $M_\odot$ and a maximum core radius of 7 km. For the reasons stated in Section 3.1.1 we will assume a slightly more conservative maximum breaking strain than that for normal neutron stars of $\sigma_{\max} = 10^{-2}$. This gives a maximum quadrupole (for $\Delta = 50$ MeV, $\mu_q = 500$, $\mu = 97\,\mathrm{MeV\,fm^{-3}} \approx 1.5 \times 10^{34}\,\mathrm{J\,m^{-3}}$) of $Q_{\max} \approx 1.4 \times 10^{36}\,\mathrm{kg\,m^2}$, or almost three orders of magnitude larger than a *normal* neutron star, which is not necessarily surprising since deformations are in the high-density core rather than the crust. Haskell et al. (2007) note that for a star with a fluid envelope around the core the quadrupole will be suppressed, particularly if there is not a substantial change in density when transitioning between the core and envelope. Converting this to an approximate estimate of the ellipticity, by assuming the canonical moment of inertia, would give an equivalently large $\varepsilon \approx 0.02$!

[6] Mannarelli et al. (2007) give a range from $5 \leq \Delta \leq 25$ MeV, although Knippel & Sedrakian (2009) suggest that for the low-temperature CCS phase appropriate for these cores larger gap values, maybe up to 100 MeV, are possible.

3.1.3 Hybrid and meson condensate stars

Owen (2005) also looks at hybrid stars with charged meson condensates and quark-baryon cores. For these the shear modulus is given by

$$\mu = 0.25\,\mathrm{MeV\,fm^{-3}}\,q_{0.4}^2 D_{15}^6 S_{30}^{-4}, \tag{7}$$

where $q_{0.4}$ is the charge density of quark droplets in units of $-0.4e$, D_{15} is their diameter in units of 15 fm and S_{30} is their spacing in units of 30 fm. Following the correction for charge screening in Owen (2005) an upper limit on shear modulus is given as $\mu \approx 1.3 \times 10^{-2}\,\mathrm{MeV\,fm^{-3}}$. If we evaluate equation (4) with this, again substituting for the core radius (which as in Section 3.1.2 we will set as 8 km) and using a fiducial stellar mass of 1.4 $M_\odot$ and a maximum breaking strain of $\sigma_{\max} = 10^{-2}$, we get an upper limit on the quadrupole moment of $Q_{\max} \approx 3.5 \times 10^{32}\,\mathrm{kg\,m^2}$. This is less than the extremal value for a *normal* neutron star. The work by Kurkela et al. (2010a,b) into cold quark matter suggest that hybrid stars (with pure phases of hadronic and quark matter) could have masses up to $\sim$2.1 $M_\odot$ and radii of $\sim$13 km although these are likely to have only a tiny quark core, i.e. they will mainly look like a normal hadronic neutron star. However, they show that stars with mixed phases of quarks and hadrons can have masses of up to $\sim$1.9 $M_\odot$ and radii of $\sim$11 km, which with the above assumptions allows larger quadrupole moments of $Q_{\max} \approx 1.8 \times 10^{33}\,\mathrm{kg\,m^2}$, comparable to the maximum obtainable for a *normal* neutron star (although requiring a smaller breaking strain). Converting this to an approximate ellipticity, assuming the canonical moment of inertia, would give $\varepsilon \approx 2 \times 10^{-5}$.

3.1.4 Solid strange stars

In Xu (2003) the possibility is presented that neutron stars could be made of solid strange quark matter. Xu (2003) uses the observation of kHz quasi-periodic oscillations (QPOs) in X-ray bursts from neutron stars in X-ray binaries, and their potential association with torsional modes in the star, to give a shear modulus for solid strange stars of $\mu \approx 4 \times 10^{31}\,\mathrm{J\,m^{-3}}$. As pointed out by Owen (2005) the identification of the QPO frequencies with torsional modes is somewhat problematic, but similarly we will take this shear modulus to be an upper limit for strange stars. Also Lin (2007) notes that the theoretical arguments for solid strange stars are less robust than those for the crystalline CSS discussed in Section 3.1.2. The masses and radii for models of strange quark stars can be seen, for example, in fig. 2 of Lattimer & Prakash (2001). Although these may not necessarily hold for *solid* strange stars, we will use the range of masses from 0.5 to 2 $M_\odot$ and radii from 8 to 11 km given by this figure to estimate the likely range of quadrupoles from equation (4). Unlike a *normal* neutron star models of quark stars show a decrease in mass with a decrease in radius. Using the maximum mass and radius and a breaking strain of $\sigma = 10^{-2}$ gives the highest quadrupole of $Q_{\max} \approx 3.5 \times 10^{34}\,\mathrm{kg\,m^2}$. Converting this to an approximate ellipticity, assuming the canonical moment of inertia, would give $\varepsilon \approx 5 \times 10^{-4}$.

4 LIMITS FROM DETECTION

The spin-down limit assumes that the total spin-down luminosity of the pulsar is emitted as gravitational radiation, but if we assume that the currently known pulsars are only *just* observable at an S/N of 5 we can estimate what *angle averaged* percentage of the spin-down power is going into the gravitational wave emission. This is shown for ALV, ET-B and ET-C in Fig. 9. We can see that for the majority of pulsars for which we could beat the spin-down limit more than 1 per cent of the spin-down power would need to be lost via gravitational waves for us to just observe them (with only 12 per cent, 26 per cent and 34 per cent requiring less than this for ALV, ET-B and ET-C, respectively). Less than 1 per cent would be consistent with the one pulsar for which we have a reliable limit on this for (the Crab pulsar) that is losing less than 2 per cent of its power in this way (Abbott et al. 2010). However, for the majority of pulsars we have no reliable way to estimate how much energy is lost via gravitational waves, especially given that only a few *young* pulsars (and no millisecond pulsars) have measured braking indices, so tens of per cent are not ruled out.

As we saw in Section 3 there are large uncertainties in many of the parameters that give rise to a neutron star's quadrupole moment. The stars could also just be intrinsically quite un-strained, i.e. $\langle \sigma_{22} \rangle$ may just be small. This, and the fact that many parameters are highly correlated, means that gravitational wave observations from the quadrupole of a triaxial neutron star will generally be unable to pin-down much of the physics giving rise to it. However, as we have seen in Section 3 there are reasonably hard upper limits on the emission allowable for stars with different EoS, so if we see emission above a particular EoS limit then these observations could rule that out for a particular pulsar, or alternatively rule others in.

With this in mind we will look at all currently known pulsars within the expected sensitive bands of ALV and the ET (in ET-B and ET-C configurations) and say whether they could be constrained to a particular EoS, or whether a variety of EoS are valid. We will do this for pulsars that the spin-down limit suggests are observable with an S/N of 5 or greater. However, it should be noted that our list of EoS is not exhaustive, and other possibilities may exist (whether they have already been theorized or not), so here constraining a pulsar to a particular EoS may not be the end of the story.

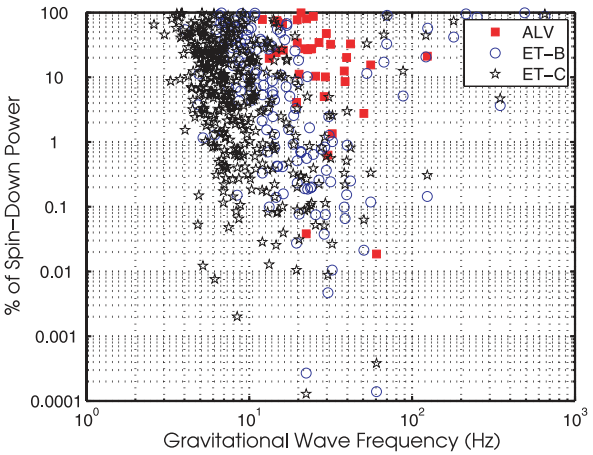

Figure 9. The percentage of the spin-down power of known pulsars emitted via gravitational waves if the pulsar is just observable with an S/N of 5. Squares represent observation with ALV, circles represent ET-B and stars represent ET-C.

The quadrupole moments for each pulsar that could be observed with ALV, ET-B and ET-C are shown in Fig. 10, both for the case that the pulsar is emitting at its spin-down limit and also an angle averaged scaled value that assumes the pulsar is only *just* observable

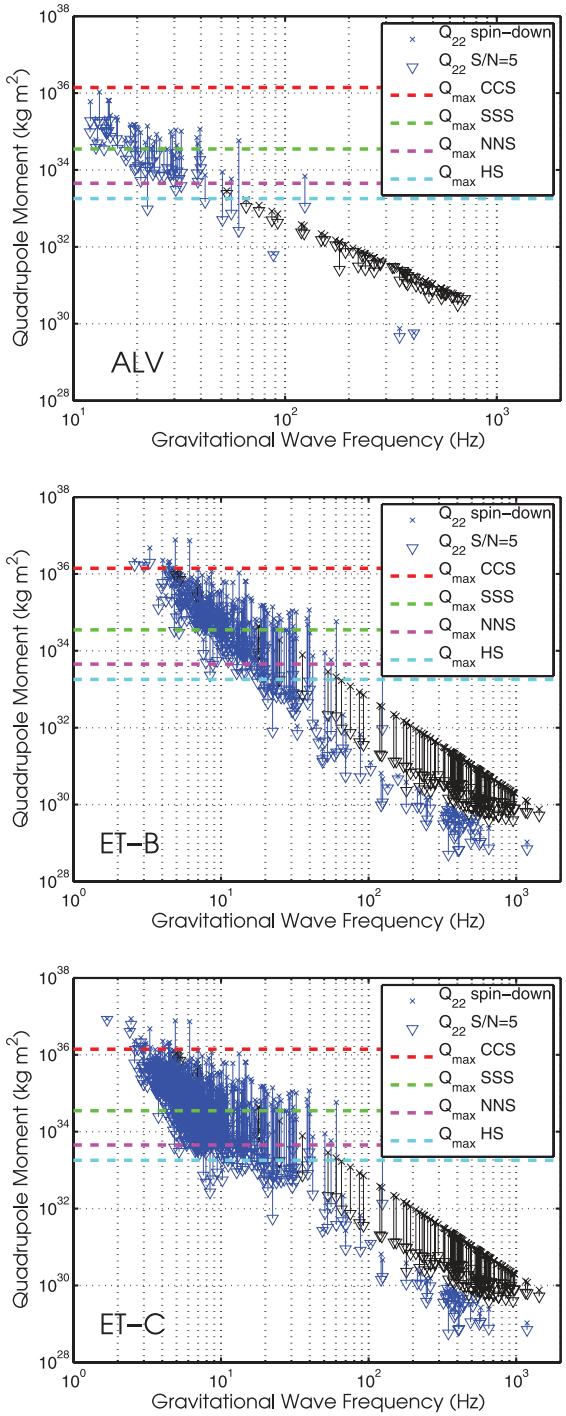

Figure 10. Necessary quadrupole moments of known pulsars, based on spin-down limits, for them to be observable with (from top to bottom) ALV, ET-B and ET-C. Limits based on the observed spin-down, or a spin-down of $\dot{\nu} = -5 \times 10^{-13}\,\mathrm{Hz\,s^{-1}}$ for GC pulsars, are given as crosses (blue for non-GC pulsars and black for GC pulsars). Angle averaged quadrupole values based on emission at an S/N of 5 are given as triangles. The approximate maximum quadrupoles from the various EoS discussed in Section 3 are also plotted.

at an S/N of 5 (the scaling factor for each pulsar can be obtained by taking the square root of the values from Fig. 9). Maximum values for the different EoS taken from Section 3 are also shown. The values are calculated from known spin-down limits, which are not available for GC pulsars, so for these we have limits based on two assumptions. The first is a spin-down-based limit that assumes (see Section 4.1) that the star has a maximal gravitational wave spin-down of $\dot{\nu} = -5 \times 10^{-13}$ Hz s^{-1}, and the second is, as above, assuming that the star is observable at an S/N of 5. As shown in Section 4.1 the values of h_0 needed to produce the levels of emission required for this S/N can be converted into equivalent gravitational wave spin-down values. For ALV about half, and for ET-B/C all bar one of the pulsars (see Fig. 12), are well within a range that could be masked by intra-cluster accelerations (we exclude the others). The number of pulsars with angle averaged quadrupoles below the spin-down limits for ALV, ET-B and ET-C are 59, 295 and 624, respectively (or 77, 408 and 774, respectively, for the best case orientation, and 50, 408 and 531 for the worst case orientation). Note that due to the reasons discussed in Section 2.1, these numbers are not quite the same as those suggested from an angle averaged S/N.

From Fig. 10 (summarized in a histogram form in Fig. 11) we see that for the vast majority of young pulsars (generally those below ~40 Hz) the S/N limits correspond to large quadrupoles only supportable by the most extreme EoS mainly through the application of a large breaking strain. We unfortunately cannot expect the majority of these quadrupoles to be realistic unless there is a very unexpected large population of highly deformed stars. However, this could be realistic for a small subset of these pulsars, or some as yet undiscovered sources.

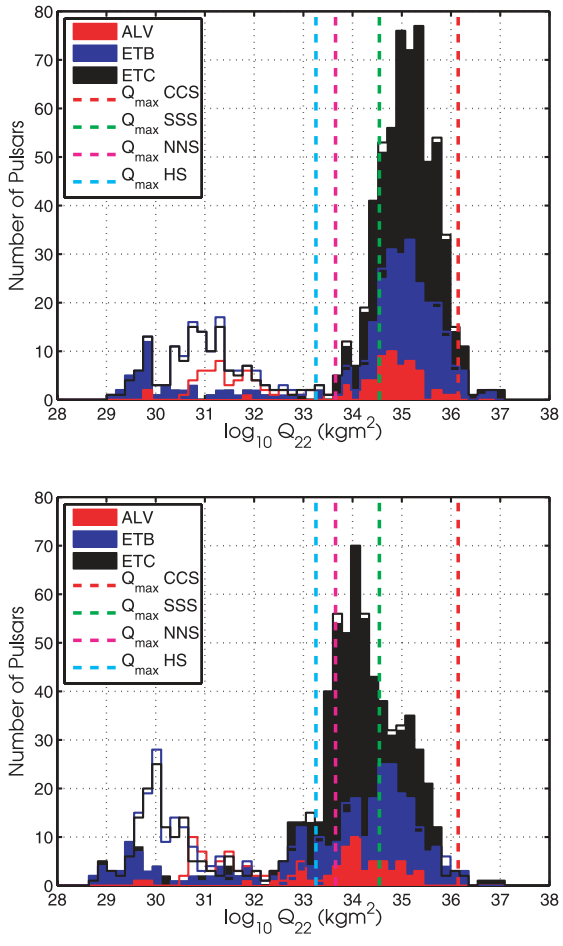

Figure 11. Quadrupole moments of known pulsars (Fig. 10), for them to be observable with ALV, ET-B and ET-C if emitting at the spin-down limit (top) and if scaled as to be *just* observable at an S/N of 5 (bottom). The filled histograms show just those pulsars outside of GCs and the unfilled histograms also include pulsars within GCs.

It should be stressed that these pulsars could however all be very smooth. The spin-down limits alone in Fig. 10 show that the lowest quadrupoles are only a few 10^{29} kg m^2 (or converting to ellipticities a few 10^{-9}) and all pulsars could be at or below this level. However, even at this low level Fig. 10 shows that these may be detectable at S/N of a few with ET.

A summary of the total numbers of pulsars below each EoS limit for pulsars within, and outside, GCs is given in Table 3.

4.1 Spin-down limits for globular cluster pulsars

Several GCs have been specifically targeted in radio searches for millisecond pulsars due to having a large population of old stars. This has led to a selection effect giving large numbers of the currently known pulsars residing in GCs. Pulsars within a GC will undergo significant accelerations, which contaminate their true spin-down rate $\dot{\nu}_{\rm int}$ via

$$\dot{\nu}_{\rm obs} = \dot{\nu}_{\rm int} - \frac{a_{||}}{c}\nu, \tag{8}$$

where $\dot{\nu}_{\rm obs}$ is the observed spin-down, ν is the pulsar frequency and $a_{||}$ is the pulsar's acceleration along the line of site – in fact many are observed to have a spin-up due to the accelerations (as they are millisecond pulsars they have small intrinsic spin-downs anyway, so it is quite easy for the accelerations to swamp this value). We can therefore use gravitational wave observations of this set of pulsars, through either upper limits or detections, to set limits on the gravitational wave component of the intrinsic spin-down rate via

$$\dot{\nu}_{\rm GW} = -h_0^2 \left(\frac{2c^3 r^2 \nu}{5GI_{zz}} \right). \tag{9}$$

We cannot, however, limit the overall spin-down as, unless the stars' acceleration can be independently assessed and the observed spin-down calculated, there is no way to know what fraction of the total spin-down is due to gravitational wave emission. As stated in Owen (2006) by looking at the observed spin-downs given for GC pulsars in the Australia Telescope National Facility (ATNF) Pulsar Catalogue (Manchester et al. 2005) it would be hard for cluster dynamics to mask spin-downs larger than $\dot{\nu} \sim -5 \times 10^{-13}$ Hz s^{-1} (this being the largest observed spin-up seen for any GC pulsar), so if gravitational wave observations can limit values to smaller than this, then results could be providing new information.

In Fig. 12 the values of the gravitational wave spin-down that the GC pulsars would require to be observed at S/N of 5 are given. For ALV 52 of the 103 observable GC pulsars, and for ET-B and ET-C 1 of the 107 observable pulsars, would need spin-downs greater than -5×10^{-13} Hz s^{-1}, i.e. values that probably could not be masked by accelerations and therefore would already be seen as having large spin-downs from radio observations. For the rest of the pulsars the spin-downs they would need could relatively easily be masked by accelerations, so they are definitely worthwhile as targets for gravitational wave searches.

These limits are the smallest values that the spin-down could have to be observable, but for many of these pulsars there is a 1–2 orders of magnitude range between these limits and the (observationally motivated, but slightly arbitrary) maximum limit of $\dot{\nu} \approx -5 \times$

Table 3. Summary of the quadrupole moment limits given in Figs 10 and 11. For comparison the total number of non-GC pulsars with angle averaged quadrupoles below the spin-down limit and observable with an S/N >5 are 59, 295 and 624 for ALV, ET-B and ET-C, respectively. The total number of GC pulsars potentially observable with S/N > 5 and a spin-down limit smaller than $-5 \times 10^{-13}\,\mathrm{Hz\,s^{-1}}$ is 51 and 106 for ALV and ET-B/C, respectively.

		Number of pulsars below limit			
		$Q_{\max}$ CCS	$Q_{\max}$ SSS	$Q_{\max}$ NNS	$Q_{\max}$ HS
ALV	Spin-down limit	59	17	3	3
	S/N = 5	59	42	11	9
	GC spin-down limit ($\dot{\nu} = -5 \times 10^{-13}\,\mathrm{Hz\,s^{-1}}$)	51	51	51	50
	GC S/N = 5	51	51	51	50
ET-B	Spin-down limit	286	90	53	51
	S/N = 5	292	175	103	85
	GC spin-down limit ($\dot{\nu} = -5 \times 10^{-13}\,\mathrm{Hz\,s^{-1}}$)	106	101	99	97
	GC S/N = 5	106	103	101	101
ET-C	Spin-down limit	605	131	43	41
	S/N = 5	618	421	152	93
	GC spin-down limit ($\dot{\nu} = -5 \times 10^{-13}\,\mathrm{Hz\,s^{-1}}$)	106	101	99	97
	GC S/N = 5	106	104	102	101

$10^{-13}\,\mathrm{Hz\,s^{-1}}$. So, there is quite a lot of leeway for these pulsars to be emitting at greater levels than that producing an S/N of 5. Also, it can be seen from Fig. 10 that for the majority of these pulsars, both the maximum and minimum observable quadrupoles are in ranges allowable by all equations of state.

4.2 Limits on magnetic fields

Deformations of a neutron star can be supported purely by the strain that the star can sustain,[7] although the mechanism giving rise to this strain may be unknown. However, magnetic fields give both a mechanism for producing strains and a way of sustaining that strain. The external magnetic fields of most pulsars can be estimated by assuming that all spin-down is due to magnetic dipole radiation, and these show that for millisecond pulsars the magnetic field strengths are comparatively small (10^8 to 10^9 G) and nowhere near enough to sustain an appreciable deformation on the star. The young pulsars have external dipole fields about 1000 times larger at $\sim 10^{12}$ G, but this is generally still not enough to give deformations that would produce observable gravitational waves. However, these stars could potentially have internal fields far larger than the external dipole, which would be large enough to give rise to gravitational wave producing distortions. As done in Abbott et al. (2010), we can use gravitational wave observations, or upper limits, to place limits on this internal field strength for all the currently known pulsars. Cutler (2002) predicts that in *normal* neutron stars toroidal magnetic fields could give rise to prolate stars with ellipticities of the order of

$$\varepsilon = 1.6 \times 10^{-6} \times \begin{cases} \langle B_{15} \rangle \mathrm{G}, & B < 10^{15}\,\mathrm{G}, \\ \langle B_{15}^2 \rangle / \mathrm{G}^2, & B > 10^{15}\,\mathrm{G}, \end{cases} \tag{10}$$

where $\langle B_{15} \rangle$ is the volume averaged magnetic field in units of 10^{15} G. Haskell et al. (2008) also study the role of internal magnetic fields, both entirely poloidal and toroidal, and how this would affect the star's ellipticity (in particular for a star with an EoS described by an $n = 1$ polytrope). They give

$$\varepsilon \approx R_{10}^4 M_{1.4}^{-2} \langle B_{15}^2 \rangle \times \begin{cases} 2 \times 10^{-4}, & \text{poloidal}, \\ -1 \times 10^{-6}, & \text{toroidal}, \end{cases} \tag{11}$$

which for the toroidal case is similar to that of Cutler (2002). Very similar limits for toroidal fields in superconducting stars are given by Akgün & Wasserman (2008). These equations can be re-arranged to give limits on the magnetic fields given gravitational wave observations of the quadrupole (see Section 3) and an assumed moment of inertia, which here we will take as $10^{38}\,\mathrm{kg\,m^2}$ (as noted above this is probably a lower limit and could differ by up to a factor of $\sim$3). Potential measurements of the field strength for both the poloidal and toroidal cases if signals were observed at an S/N of 5 for the ALV, ET-B and ET-C set ups are given in Fig. 13.

We can see that for the young pulsars (with frequencies $\lesssim$40 Hz) internal magnetic fields of greater than 10^{14} G would be required to observe them, which is of a similar strength to the *external* fields of a magnetars at 10^{14}–10^{15} G. For the millisecond pulsars, in particular the non-GC pulsars, internal poloidal fields of a few 10^{12} G could provide observable signals, although if there are only toroidal fields then a couple of orders of magnitude higher would be necessary. Of course, the field geometry could be complex and a combination of toroidal and poloidal components and the calculations above rely on a specific EoS.

5 DISCUSSION

We have looked at our ability to detect and estimate parameters from gravitational wave observations for known (non-accreting) pulsars. Using Bayesian hypothesis testing, we estimate that signals with an S/N of 5 could be detected with 95 per cent efficiency. This assumes that the data are Gaussian, and experience of real detector data shows that this assumption can be reasonable on short time-scales and with effectively cleaned data, although there will still probably be some small degrading of detection ability.

Once detected, we have shown how estimates of various parameters will be affected as signals increase in S/N, and also how the pulsar's orientation affects this. We see that for strong signals in

[7] How long such a deformation could be sustained due to visco-elastic creep smoothing it out is something that needs further study, e.g. Chugunov & Horowitz (2010) who suggest short time-scales of a few years for hot stars, but far longer for cooler stars (although they note extrapolations to lower temperatures and longer time-scales must be treated with care).

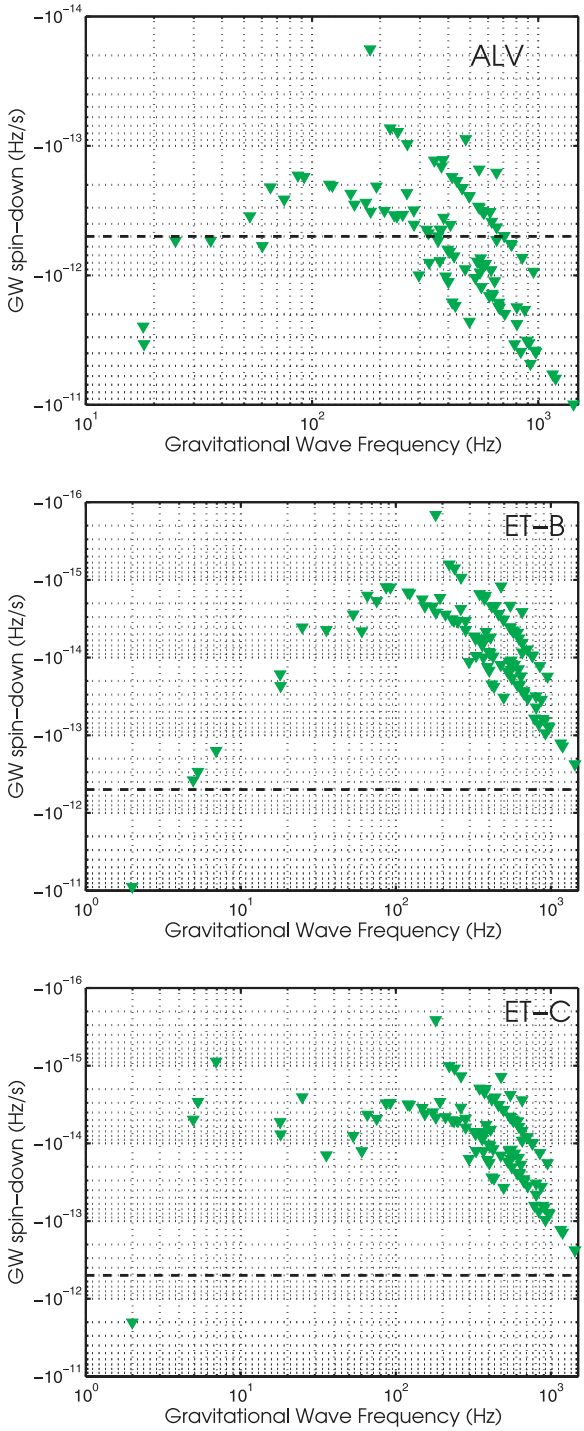

Figure 12. Spin-downs that would be needed in currently known GC pulsars for them to be observed with (from top to bottom) ALV, ET-B and ET-C at an S/N of 5.

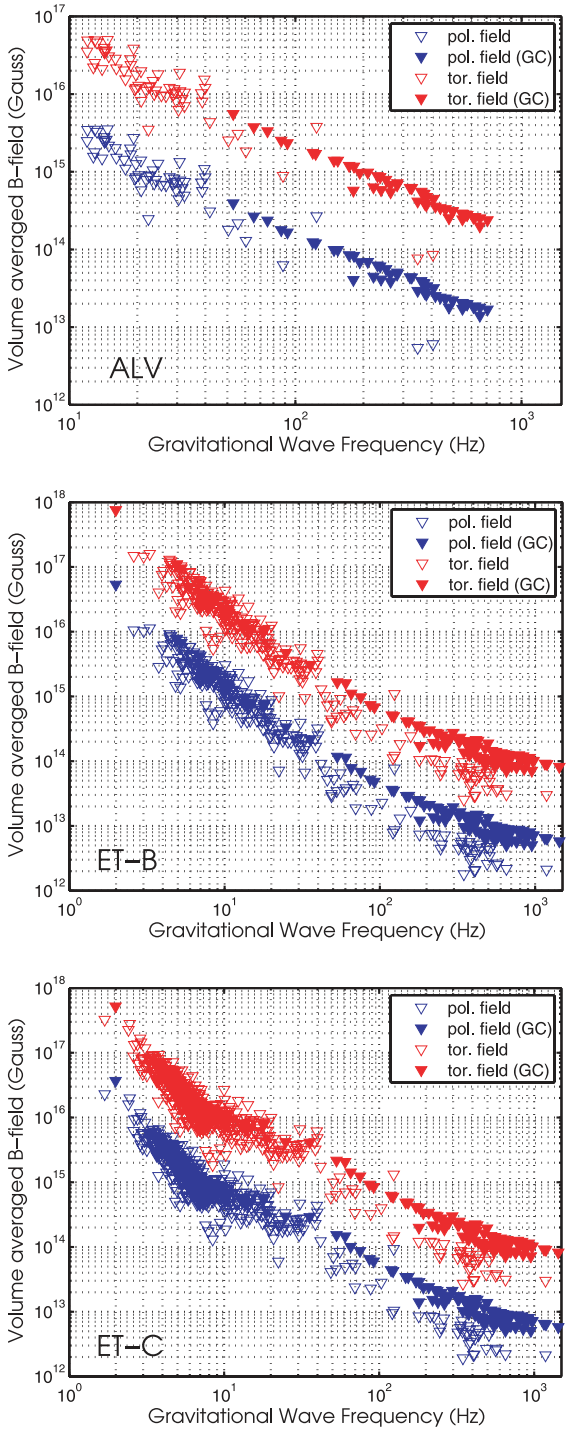

Figure 13. Potential internal magnetic field strengths that would be needed in currently known pulsars to observe them with an S/N of 5 with (from top to bottom) ALV, ET-B and ET-C.

the case where the orientation is most favourable and gives a larger S/N (i.e. the gravitational waves are circularly polarized) the uncertainty on the gravitational wave amplitude will actually be larger than an equivalent amplitude source with a worse orientation. So, when detections become regular the best parameter constraints will actually be made for the linearly polarized sources. However, we also see that unless the distance to these pulsars can be measured to better than ∼10 per cent then the fractional error on the quadrupole calculated from the gravitational wave amplitude will be relatively insensitive to the orientation, because the uncertainty is dominated by the distance uncertainty.

We have seen the sorts of mass quadrupoles that would be necessary to observe the set of currently known pulsars with future gravitational wave observatories, and compared these to maximum theoretical predictions for a variety of EoS. As has previously been noted many times (e.g. Abbott et al. 2007a) for the majority of

millisecond pulsars, if we are able to beat their spin-down limits and observe them, the quadrupoles (or ellipticities) they would have are sustainable by all EoS and would therefore not be able to constrain the type of matter in the star. However, with observations of many pulsars useful population statistics could be obtained and potential differences between different populations explored (e.g. GC pulsar and non-GC pulsars). To be observed with ALV, ET-B or ET-C the majority of young pulsars (with frequencies $\lesssim$40 Hz) would have to have quadrupoles greater than $\approx 10^{33}$ kg m^2, which would only be sustainable for highly strained crystalline CSSs or solid strange quark stars. Therefore, if such stars were observed it would provide a great deal of insight into neutron star matter. The number of pulsars potentially observable at an S/N of 5, and consistent with being a *normal* neutron star, is 11 for ALV, 103 for ET-B and 152 for ET-C. It is important to note that this does not mean that they *will* have these quadrupoles and they could all be smoother than our limits are able to set.

In Andersson et al. (2011), which studies the prospects of observing gravitational waves from neutron stars with ET (in particular the ET-B configuration), they take the assumption that realistic stars would optimistically have ellipticities $<10^{-7}$ and conclude that only some of the hundreds of millisecond pulsars currently known would be potentially observable. From this work we can look at the number of known pulsars we might expect to be observable at an S/N greater than 5 given that they are losing less than a specific percentage of their spin-down power through gravitational wave emission, and have quadrupoles below specific levels (this is shown in Table 4). We find that for ALV if we take pulsars that would only need to be emitting less than 50 per cent of their spin-down luminosity via gravitational waves to be observable at S/N of greater than 5, and had quadrupoles less than $Q_{22} < 10^{30}$–10^{31} kg m^2 (or ellipticities of $\lesssim 10^{-8}$ to 10^{-7}), then only three of the currently known pulsars would be observable. We find that none is observable if requiring these quadrupole levels and also emitting less than 10 per cent of the spin-down power via gravitational waves. For ET (in either ET-B or ET-C configurations) if we take pulsars which would only need to be emitting less than 10 per cent of their spin-down luminosity, and with quadrupoles $<10^{30}$–10^{31} kg m^2, then 6–11 currently known pulsars would be observable, respectively. For the one pulsar that we can currently calculate a limit on the spin-down power we see that less than 2 per cent of the spin-down luminosity is emitted via gravitational waves, so using this as a guide and taking only pulsars that could emit less than 1 per cent of their spin-down power in gravitational waves and still be observable (and with the above quadrupoles) we find only one pulsar. These numbers are based on currently known pulsars and use only the non-GC pulsars; for the millisecond pulsars that these results represent (due to the small quadrupole requirements) approximately half are within GCs, so assuming there is no difference in spin-downs between GC and non-GC populations of pulsars then the number of observable pulsars could double. Also, as stated in Section 2, future radio telescopes such as the SKA could observe $\approx$1000 millisecond pulsars increasing the current number by a factor of 5. This could give tens of observable pulsars for ET.

Table 4. The number of pulsars potentially observable given gravitational wave emission consuming less than various percentages of the total spin-down power, and requiring quadrupoles less than the given values.

	Number of pulsars			
Q_{22} kg m^2 <	10^{33}	10^{32}	10^{31}	10^{30}
$\varepsilon \lesssim$	10^{-5}	10^{-6}	10^{-7}	10^{-8}
Per cent of spin-down power		<100 per cent		
ALV	8	5	4	1
ET-B	51	45	37	27
ET-C	40	38	33	25
Per cent of spin-down power		<50 per cent		
ALV	5	3	3	1
ET-B	37	32	27	19
ET-C	28	26	23	15
Per cent of spin-down power		<10 per cent		
ALV	*	*	*	*
ET-B	15	13	11	6
ET-C	12	10	9	6
Per cent of spin-down power		<1 per cent		
ALV	*	*	*	*
ET-B	2	2	1	1
ET-C	1	1	1	1

We see that for many millisecond pulsars, if they have internal poloidal magnetic fields similar in strength to the external fields of young pulsars, or toroidal field similar in strength to the external field of magnetars, then they may sustain ellipticities that make them observable. In reality, the internal field will probably consist of both poloidal and toroidal components. Young pulsar would require far higher magnetic fields for them to sustain ellipticities that would allow them to be observable.

The above estimates have all assumed a year of observation. However, the future detectors could run over several years, and the third-generation detectors may even be the premier gravitational wave observatories spanning decades. There could also be other similarly sensitive detectors added to the network (e.g. the LCGT). All of these would increase the ability to make observations of, and hopefully refine parameter estimation for, known pulsars, although the scaling of these improvements (for equivalent detectors) will only be the square root of the observation time. Better prospects could come from a far larger selection of pulsar targets from future radio/X-ray/γ-ray surveys.

One of the main points to note here is that all the above calculations have significant uncertainties to them. The theoretical study of neutron star EoS is still an area of study with large uncertainties. Neutron star mass measurements currently seem to favour fairly conventional EoS, and our upper limits for these may be a fair representation of reality. However, the current crop of known pulsars may harbour a variety of stellar types and our observations may be the only way to differentiate between them. More theoretical understanding through simulations of maximum breaking strains of quark matter and hybrid star matter would be of great help in making these constraints. In addition to determining whether a star is physically capable of supporting an observably large strain, it is of great importance for future studies to find mechanisms of producing and sustaining such strains.

The study here has also assumed emission from a triaxial neutron star emitting at precisely twice the observed electromagnetic frequency via the Q_{22} mass quadrupole. Potentially more interesting physics could be extracted if the gravitational wave signal and electromagnetic signal were not so closely aligned (e.g. if pulsar timing noise is only present in the electromagnetic signal; Jones 2004; Pitkin & Woan 2007). Deviations between the two could uncover information about the coupling of the gravitational wave producing component and electromagnetic-producing component, and

emission may occur at the rotation rate (Jones 2010). Also, gravitational waves from other vibrational modes, such as long-lived *r* modes (Arras et al. 2003; Owen 2010), or fundamental modes (possibly excited by glitches), may be able to tell us far more about the neutron star EoS.

ACKNOWLEDGMENTS

This work has been funded under a UK Science and Technology Facilities Council rolling grant. I am very grateful to many members of the LIGO Scientific Collaboration and Virgo Collaboration continuous wave search group for useful discussions and suggestions on the issues in this paper, and for reading through early drafts. In particular, I would like to thank Graham Woan, Ian Jones, Ben Owen and Keith Riles for their comments. I would also like to thank Roy Smits for the useful information he provided.

REFERENCES

Abadie J. et al., 2010, Nuclear Instruments Methods Phys. Res. A, 624, 223
Abadie J. et al., 2011, preprint (arXiv:1104.2712v2)
Abbott B. P. et al., 2004a, Nuclear Instruments Methods Phys. Res. A, 517, 154
Abbott B. P. et al., 2004b, Phys. Rev. D, 69, 082004
Abbott B. P. et al., 2005, Phys. Rev. Lett., 94, 181103
Abbott B. P. et al., 2007a, Phys. Rev. D, 76, 042001
Abbott B. P. et al., 2007b, Phys. Rev. D, 76, 082001
Abbott B. P. et al., 2008a, ApJ, 683, L45
Abbott B. P. et al., 2008b, Phys. Rev. D, 77, 022001
Abbott B. P. et al., 2009a, Rep. Progress Phys., 72, 076901
Abbott B. P. et al., 2009b, Phys. Rev. Lett., 102, 111102
Abbott B. P. et al., 2009c, Phys. Rev. D, 79, 022001
Abbott B. P. et al., 2010, ApJ, 713, 671
Acernese F. et al., 2008, Class. Quantum Grav., 25, 184001
Akgün T., Wasserman I., 2008, MNRAS, 383, 1551
Andersson N., Kokkotas K. D., 1998, MNRAS, 299, 1059
Andersson N, Ferrari V, Jones D. I, Kokkotas K. D., Krishnan B., Read J., Rezzolla L., Zink B., 2011, Gen. Relativ. Gravitation, 43, 409
Ando M., The TAMA Collaboration, 2005, Class. Quantum Grav., 22, 18, S881
Arras P., Flanagan E. E, Morsink S. M., Schenk A. K., Teukolsky S. A., Wasserman I., 2003, ApJ, 591, 1129
Chugunov A. I., Horowitz C. J., 2011, MNRAS, 407, L54
Clark J., Heng I. S., Pitkin M., Woan G., 2007, Phys. Rev. D, 76, 043003
Cordes J. M., Lazio T. J. W., 2002, preprint (astro-ph/0207156)
Cordes J. M., Kramer M., Lazio T. J. W., Stappers B. W., Backer D. C., Johnston S., 2004, New Astron. Rev., 48, 1413
Cutler C., 2002, Phys. Rev. D, 66, 084025
Dupuis R. J., Woan G., 2005, Phys. Rev. D, 72, 102002
Flanagan É. É., Hinderer T., 2008, Phys. Rev. D, 77, 021502
Freise A., Hild S., Somiya K., Strain K., Vicere A., Barsuglia M., Chelkowski S., 2009, Gen. Relativ. Gravit. (doi:10.1007/s10714-010-1018-2) (arXiv:0908.0353v1)
Harry G., The LIGO Scientific Collaboration, 2010, Class. Quantum Grav., 27, 084006
Haskell B., Jones D. I., Andersson N., 2006, MNRAS, 373, 1423
Haskell B., Andersson N., Jones D. I., Samuelsson L., 2007, Phys. Rev. Lett., 99, 231101
Haskell B., Samuelsson L., Glampedakis K., Andersson N., 2008, MNRAS, 385, 531
Hild S., Chelkowski S., Freise A., 2008, preprint (arXiv:0810.0604v2)
Hild S., Chelkowski S., Freise A., Franc J., Morgado N., Flaminio R., DeSalvo R., 2010, Class. Quantum Grav., 27, 015003
Hild S. et al., 2011, Class. Quantum Grav., 28, 094013
Horowitz C. J., 2010, Phys. Rev. D, 81, 103001
Horowitz C. J., Kadau K., 2009, Phys. Rev. Lett., 102, 19, 191102
Jaranowski P., Królak A., 2010, Class. Quantum Grav., 27, 194015
Jaranowski P., Królak A., Schutz B. F., 1998, Phys. Rev. D, 58, 063001
Jones D. I., 2004, Phys. Rev. D, 70, 042002
Jones D. I., 2007, Ap&SS, 308, 125
Jones D. I., 2010, MNRAS, 402, 2505
Knippel B., Sedrakian A., 2009, Phys. Rev. D, 79, 083007
Knispel B., Allen B., 2008, Phys. Rev. D, 78, 044031
Kurkela A., Romatschke P., Vuorinen A., 2010a, Phys. Rev. D, 81, 105021
Kurkela A., Romatschke P., Vuorinen A., Wu B., 2010b, preprint (arXiv:1006.4062)
Kuroda K., The LCGT Collaboration, 2010, Class. Quantum Grav., 27, 084004
Lattimer J. M., Prakash M., 2001, ApJ, 550, 426
Lattimer J. M., Prakash M., 2007, Phys. Rep., 442, 109
LIGO Scientific Collaboration, 2009, Advanced LIGO Anticipated Sensitivity Curves. LIGO-T0900288-v2, https://dcc.ligo.org/cgi-bin/DocDB/ShowDocument?docid = 2974
Lin L-M., 2007, Phys. Rev. D, 76, 081502
Manchester R. N., Hobbs G. B., Teoh A., Hobbs M., 2005, AJ, 129, 1993 http://www.atnf.csiro.au/research/pulsar/psrcat/
Mannarelli M., Rajagopal K., Sharma R., 2007, Phys. Rev. D, 76, 074026
Ng C.-Y., Romani R. W., 2008, ApJ, 673, 411
Owen B. J., 2005, Phys. Rev. Lett., 95, 21, 211101
Owen B. J., 2006, Class. Quantum Grav., 23, S1
Owen B. J., 2010, Phys. Rev. D, 82, 104002
Palomba C., 2000, A&A, 354, 163
Pitkin M, Woan G., 2007, Phys. Rev. D, 76, 042006
Prix R., Krishnan B., 2009, Class. Quantum Grav., 26, 204013
Punturo M. et al., 2010, Class. Quantum Grav., 27, 084007
Santostasi G., 2006, APS Meeting Abstracts, D1095
Seto N., 2005, Phys. Rev. D., 71, 123002
Smits R., Tingay S. J., Wex N., Kramer M., Stappers B., 2011, A&A, 528, A108
The Virgo Collaboration, 2009, AdvVirgo Baseline Design Virgo Internal Note VIR-0027A-09
Ushomirsky G., Cutler C., Bildsten L., 2000, MNRAS, 319, 902
Watts A. L., Krishnan B., Bildsten L., Schutz B. F., 2008, MNRAS, 389, 839
Will C. M., 2006, Living Rev. Relativ., 9, 3
Willke B. et al., 2006, Class. Quantum Grav., 23, S207
Xu R. X., 2003, ApJ, 596, L59

This paper has been typeset from a TEX/LATEX file prepared by the author.